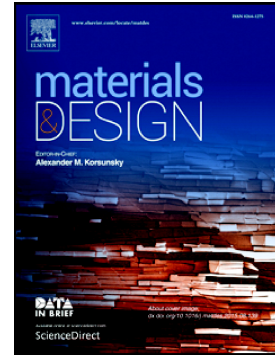# Journal Pre-proof

Enhancing fatigue performance of damaged metallic structures by bonded CFRP patches considering temperature effects

Lu Ke, Chuanxi Li, Jun He, Qiang Shen, Yongming Liu, Yang Jiao

Please cite this article as: L. Ke, C. Li, J. He, et al., Enhancing fatigue performance of damaged metallic structures by bonded CFRP patches considering temperature effects, *Materials & Design* (2020), https://doi.org/10.1016/j.matdes.2020.108731

This is a PDF file of an article that has undergone enhancements after acceptance, such as the addition of a cover page and metadata, and formatting for readability, but it is not yet the definitive version of record. This version will undergo additional copyediting, typesetting and review before it is published in its final form, but we are providing this version to give early visibility of the article. Please note that, during the production process, errors may be discovered which could affect the content, and all legal disclaimers that apply to the journal pertain.

Enhancing fatigue performance of damaged metallic structures by bonded CFRP patches considering temperature effects

Lu Ke [a,b], Chuanxi Li [a *], Jun He [a,c], Qiang Shen [d], Yongming Liu [b], Yang Jiao [b]

a. School of Civil Engineering, Changsha University of Science and Technology, Changsha 410114, China

b. School for Engineering of Matter, Transport and Energy, Arizona State University, Tempe, AZ 85287, USA

c. Institute for Infrastructure and Environment, Heriot-Watt University, Edinburgh, Currie EH14 4AS, UK

d. School of Aeronautics and Astronautics, Shanghai Jiao Tong University, Shanghai 200240, China

Abstract: This paper reports an experimental and theoretical investigation on the fatigue performance enhancement of damaged steel structures by bonded carbon fiber reinforced polymer (CFRP) systems considering the temperature effects. First, thermomechanical properties of the epoxy adhesive and CFRPs were examined via dynamic mechanical analysis (DMA) and tensile tests. The appropriate curing procedure for the structural adhesive was obtained. Next, the fatigue behavior of notched steel plates strengthened by bonded CFRPs was investigated at different temperatures. During the fatigue tests, beach marking and back-face strain techniques were used to monitor the fatigue crack growth on steel components and the damage evolution within the bonding interface. The results show that the high-temperature resistance of the epoxy adhesive can be effectively improved by increasing the curing temperature and duration. The properly cured bonded CFRP patches can effectively enhance the fatigue performance of damaged steel structures. However, and the elevated temperatures significantly degrade the fatigue behavior of the CFRP-strengthened steel components.

*Corresponding authors at: School of Civil Engineering, Changsha University of Science and Technology, Changsha 410114, China.

E-mail addresses: clkelu@stu.csust.edu.cn (L. Ke), lichx@csust.edu.cn (C. Li)

1. Introduction

The retrofitting, rehabilitation and strengthening of damaged or deteriorated metallic structure is an important subject [1-3]. Traditional strengthening methods for steel structures include crack arresting hole, improving geometric continuity, bolted and welded metallic plates, etc. [4-6]. Crack arresting hole is a simple technique; however, it is not effective in many cases, e.g., torsion-induced fatigue cracks [4]. The improving geometric continuity method aims to reduce the geometric discontinuities and eliminate the stress concentrations; however, it may lead to a reduction of structural stiffness and strength. The bolted/welded metallic plates are bulky and difficult to install. Moreover, they may cause new structural damages, heat-induced material hardening and residual tensile stresses, which may worsen the fatigue problem [6]. On the other hand, lightweight carbon fiber reinforced polymer (CFRP) has received growing interests for structural rehabilitation, due to its superior properties such as high specific strength and stiffness, excellent fatigue and corrosion resistance [3, 7-10]. The bonded CFRP system (BCS) enables a faster structural strengthening with less traffic interruption; more importantly, it will not cause new damages and thermal residual stresses to the deteriorated structures [9, 11, 12]. Therefore, the bonded CFRP has promising prospects in rehabilitating steel infrastructures [11].

Existing studies showed that the efficacy of the BCS is affected by many harsh environmental factors [13, 14]. Comparing to low temperature, humidity, ultraviolet radiation, cyclic freeze-thaw, salt fog, etc., the elevated temperature regards as the most adverse factor influencing the efficacy of the bonded CFRP system [9, 15-24]. Infrastructures such as bridges and buildings are inevitably subject to high temperatures up to 50–60℃ [15, 17]. The design is to bond CFRP with steel substrates by structural epoxy adhesives. Both the CFRP and adhesive layers are sensitive to high temperatures, [20, 25]. This is because the polymer chain crosslinking in epoxy resins is degraded by elevated ambient temperatures, leading to a deterioration in their elasticity and bonding capacity. Therefore, the temperature effects on the CFRP-strengthened structures mainly originate from the epoxy adhesive and CFRP aspects.

Previous studies have proven the effectiveness of BCS in fatigue life enhancement of steel plates [26-30], beams [31, 32], bridges [33, 34], under-water structures [35, 36], etc. However, few focused on the fatigue behavior of CFRP-strengthened steel structures at elevated temperatures[16, 37-40]. Feng et al. [41] studied the temperature effects on the fatigue behavior of CFRP-strengthened steel plates. They used the CFRP sheets (fabrics) as the strengthening material, but the CFRP laminates have been proved more effective in

extending the fatigue life of steel structures [42]. CFRP laminate is a kind of prefabricated thick plates using pultrusion or compression molding technique. It is a quite different kind of material from the CFRP sheet and possesses much higher stiffness. To effectively improve fatigue performance, it is of great importance to conduct researches on analyzing the temperature effects on the steel structures strengthened with CFRP laminates.

This study aims to investigate the fatigue behavior of CFRP-strengthened single-edge notched tension (SENT) steel plates considering the effects of elevated temperatures. To ensure the efficacy of the bonding interface at high temperatures, the mechanical behavior of the epoxy adhesive should meet the service requirements at the temperatures of 25℃–60℃. The temperature-dependent mechanical behavior of the epoxy adhesive was investigated by dynamic mechanical analysis (DMA), which helps to obtain a desired curing temperature and duration for the adhesive material. Secondly, the fatigue tests on the bare (un-strengthened) and CFRP-strengthened SENT specimens were performed at 25℃, 45℃ and 60℃. The fatigue crack propagations in the steel plates and the damage within the bonding interface were monitored using the "beach marking" and "back-face strain" techniques during the tests. The failure modes, fatigue crack growth, fatigue life enhancement, and CFRP/steel interfacial debonding were evaluated base on test results. Some valuable conclusions are drawn in this study to promote the applications of CFRPs in the rehabilitation of metallic structures.

2. Material testing

2.1. Epoxy Adhesive

The bond strength of epoxy adhesive degrades dramatically when the ambient temperature approaches or exceeds the glass transition temperature. Therefore, selection of the proper adhesive and curing procedure are very important. The epoxy adhesive called J133Y, widely used in the aerospace and automotive industry, is adopted in the study. The mechanical properties can be found in Table 1. To determine the proper curing procedure of the adhesive. we conducted DMA tests for the adhesive specimens cured at different temperatures and durations according to ASTM E1640-18 [43]. The DMA tests were conducted from 0℃ to 120℃, at a frequency of 1 Hz and a heating rate of 2℃/min.

Fig. 1 depicts the DMA results of the adhesive J133Y cured with different procedures. Fig. 1(a) shows the storage moduli, E', as a function of temperature for the adhesive cured with different options. It shows that the moderately high-temperature curing can effectively enhance the high-temperature resistance of the adhesive. Extending the curing duration also

3

contributes to the enhancement of high-temperature performance of the adhesive. Since the investigated temperature in this study ranges from 25℃ to 60℃, the mechanical properties of the adhesive should be ensured within this temperature range. It is found only three curing options can maintain its storage modulus at 60℃, i.e. being cured at 80℃ for 90 min, 100℃ for 60 min and 100℃ for 90 min. To shorten the curing duration, we finally chose to cure the adhesive layers at 100℃ for 60 min for the specimen fabrication.

Fig. 1(b) shows the loss modulus, E'' of the adhesive cured at 100℃ for 1h as a function of temperature. Generally, the temperature at the tangent line intersection of the storage modulus curve is recommended as the glass transition temperature, T_g. Occasionally, the temperature at the peaks of loss modulus and loss factor curves, i.e. T_l and T_t, are sometimes used as the glass transition temperature [9, 44]. As shown in this figure, the values of T_g, T_l and T_t for the adhesive cured at 100℃ for 1h are respectively 60℃, 68℃ and 83℃, which are equal to or above the highest testing temperature considered in this study.

Fig. 1(c) and (d) demonstrate the T_g, T_l and T_t values for the adhesive cured for different durations at 80℃ and 100℃, respectively. As shown in these figures, the values of T_g, T_l and T_t for the adhesive increase with the curing duration at either 80℃ or 100℃, but the increase rate declines as the temperature increases. Moreover, the values of T_t are higher than those of T_l, followed by T_g. It also found that the higher temperature can effectively shorten the curing duration.

Table 1

Material properties of CFRP, epoxy adhesive and steel at room temperature.

Materials	Young's modulus (GPa)	Yield strength (MPa)	Tensile strength (MPa)	Elongation (%)	Poisson's ratio
CFRP (F1.4 /F3.0) [*]	161.2/ 166.9	–	2263/ 2403	1.65/ 1.53	0.25/ 0.23
Adhesive (J133Y) [*]	1.9	–	26.2	1.53	0.29
Steel (Q345qC) [*]	200.2	461	565	31.5	0.30

* Data from tensile tests.
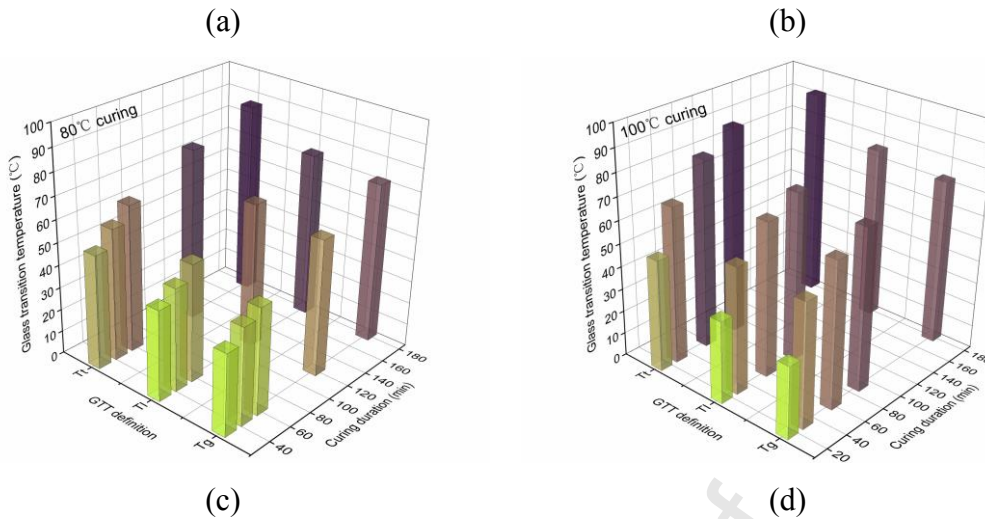
(a)   (b)

(c)   (d)
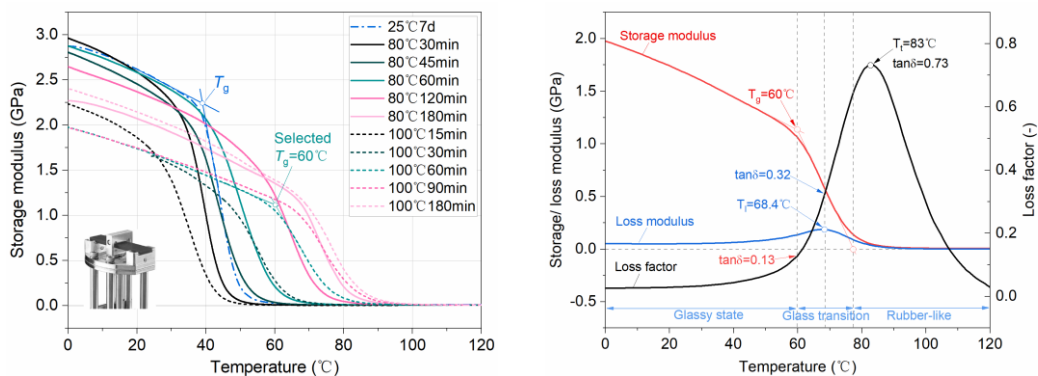
Fig. 1. DMA results of epoxy adhesive: (a) storage modulus of adhesive cured with different curing temperatures and durations;(b) storage modulus, loss modulus and loss factor of the adhesive cured at 100℃ for 1h as a function of temperature; T_g, T_l and T_t values cured at (c) 80℃ and (d) 100℃ for different durations.

The elastic and shear moduli of the epoxy adhesive cured at 100℃ for 1h are obtained by coupon tensile testing at different temperatures according to ASTM D638-14 [45], as shown in Fig. 2. The elastic and shear moduli of the epoxy adhesive decrease significantly with the increasing temperature.
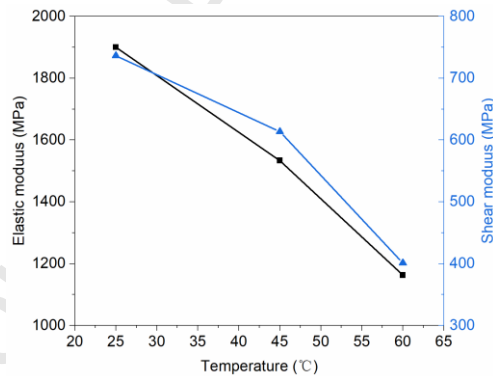
Fig. 2. Elastic and shear moduli of the epoxy adhesive cured at 100℃ for 1h as a function of temperature.

2.2. CFRP laminate

The unidirectional, one-layered CFRP laminas were used to make the CFRP/steel joints. The CFRPs are 50 mm wide and in 1.4- and 3.0-mm thicknesses (abbreviated by F1.4 and F3.0, respectively), and they are manufactured by Nanjing Hitech Co., Ltd via the pultrusion technique. The material properties of CFRP at room temperature are listed in Table 1. We also conducted tensile strength tests for the CFRP laminates at different temperatures, and the results are shown in Fig. 3. It shows that the elastic modulus of the F1.4 laminates declines slightly with the temperature increasing from 25℃ to 60℃, while that of the F3.0 laminates
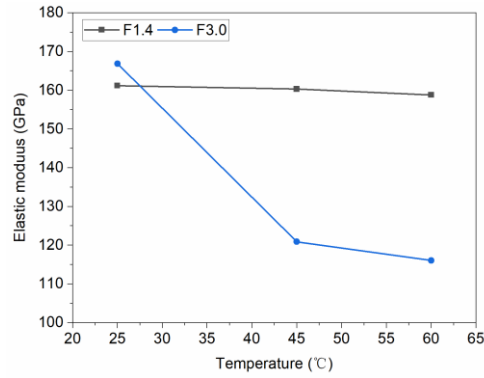
decreases significantly within this temperature range.

Fig. 3. Elastic modulus of the CFRP laminates as a function of temperature.

2.3. Steel

The steel Q345qC, which is widely applied in bridge projects in China, was used to fabricate the specimens. The mechanical properties of the steel are listed in Table 1. To obtain the fatigue crack growth parameters of steel Q345qC, We fabricated three compact tensile (CT) specimens according to ASTM E647-13a [46]. The fatigue crack growth tests were performed at a stress ratio of 0.4. The crack growth rate versus the range of stress intensity factor (SIF) (i.e. $\mathrm{d}a/\mathrm{d}N$-ΔK relationship) for the steel was depicted in Fig. 4, where the test data were fitted by the Paris Law [47, 48] described in Eqs. (1)–(3).

For the stable propagation stage of fatigue crack, the fatigue growth rate, $\mathrm{d}a/\mathrm{d}N$, can be described by the Paris Law as a function of the range of SIF, ΔK_{I}:

$$\mathrm{d}a/\mathrm{d}N = C(\Delta K_{\mathrm{I}})^{m} \tag{1}$$

where a is the crack length, and N is the number of fatigue cycles. ΔK_{I} is the range of SIF. m and C are the constant parameters for specific materials.

The range of SIF at the crack tip, ΔK, is expressed by

$$\Delta K_{\mathrm{I}} = K_{\mathrm{I,max}} - K_{\mathrm{I,min}} \tag{2}$$

where $K_{\mathrm{I,max}}$ and $K_{\mathrm{I,min}}$ are the maximum and minimum SIF in a fatigue cycle, respectively.

The Eq. (2) can be written in the base coordinate system as follows:

$$\lg(\mathrm{d}a/\mathrm{d}N) = m\lg\Delta K_{\mathrm{I}} + \lg C \tag{3}$$

In the following fatigue tests for CFRP-repaired steel specimens, the stress ratio, R =24 kN /60 kN =0.4. Therefore, the material parameters at the stress ratio of 0.4 were adopted to predict the fatigue crack growth behavior. The fatigue crack growth of steel with a stress ratio of 0.4 is shown in Fig. 4, which shows that the fatigue crack growth parameters for the steel are: C= 3.77×10^{-9}, m=3.31.
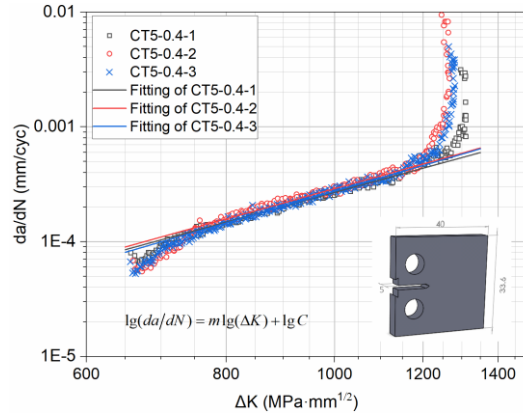
6

Fig. 4. da/dN-ΔK relationship for steel Q345qC.

3. Experimental program

3.1. Specimen details

The configuration and photo of the specimens are shown in Fig. 5. The steel plate is 260 mm long, 50 mm wide and 8 mm thick. A pre-crack notch was made on the SENT specimens by the wire-electrode cutting technique. The pre-crack notch is 6 mm long and 1.5 mm wide, and a triangular slot was made on the tip of the notch to simulate the initial crack. Detailed dimensions are shown in the local zoom-in image in Fig. 5(a). Then the SENT specimens were reinforced using double-side bonded CFRP laminates. The bonded CFRPs are 1.4 mm and 3.0 mm thick, 50 mm wide and 100 mm long. The gripping areas at both ends of the specimens are 50 mm long. The ratio of CFRP stiffness to the steel plate stiffness is defined as the reinforcement ratio, R_r:

$$R_r = \frac{2E_f A_f}{E_s A_s} \tag{4}$$

where E_f and E_s are respectively the elastic moduli of the CFRP patch and steel. A_f and A_s are the areas of the cross-section of the CFRP and steel, respectively.

The SENT specimens were fabricated in the following steps. First, the steel plates were ground to achieve a consistent roughness and cleaned carefully with acetone. Secondly, the fully mixed adhesives were pasted to the steel plates, and four steel beads with a diameter of 1.0 mm were arranged in the adhesive layer for a consistent adhesive layer thickness. Then, the CFRPs were pasted to the steel plates. Finally, all the specimens were cured at $100\pm1°C$ for 1h in an environmental chamber, except for two specimens being cured at $100\pm1°C$ for 1.5h.
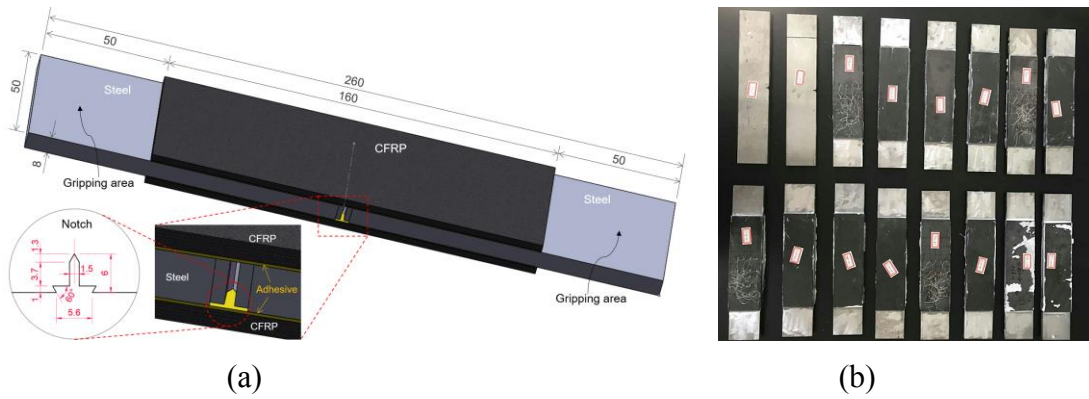
7

(a)   (b)

Fig. 5. (a) configuration and dimensions of the strengthened specimens; (b) photo of the specimens.

The test specimens can be separated into four groups as listed in Table 2. These include bare specimens, F1.4- and F3.0-strengthened specimen series. For bare specimens, the label "steel" represents the notched steel plate specimens without CFRP strengthening. For the strengthened specimens, "F1.4" and "F3.0" refer to the strengthening materials, which are respectively the 1.4 mm- and 3.0 mm-thick CFRPs. The numbers "25", "45" and "60" denote the testing temperatures. In the last series, "1.5h" represents that these specimens are cured at $100\pm1℃$ for 1.5h. These specimens are used to examine the effect of extending curing duration on fatigue strengthening.

Table 2 Details of the specimens and fatigue test results.

Series	Description	Specimen label	Reinforcement ratio	Strain measurement	Curing procedure
Bare	Bare steel specimens	Steel-1	0	No	–
		Steel-2	0	No	
F1.4	F1.4-strengthened specimens	F1.4-25-1	0.28	Yes	100℃+1h
		F1.4-25-2	0.28	No	
		F1.4-45-1	0.28	No	
		F1.4-45-2	0.28	No	
		F1.4-60-1	0.28	Yes	
		F1.4-60-2	0.28	No	
F3.0	F3.0-strengthened specimens	F3.0-25-1	0.60	Yes	100℃+1h
		F3.0-25-2	0.60	No	
		F3.0-45-1	0.60	No	
		F3.0-45-2	0.60	No	
		F3.0-60-1	0.60	Yes	
		F3.0-60-2	0.60	No	
F3.0 -1.5h	F3.0-strengthened specimens cured for 1.5h	F3.0-60-1.5h-1	0.60	No	100℃+1.5h
		F3.0-60-1.5h-2	0.60	No	

3.2. Experimental set-up

The specimens were tested under cyclic tensile loads using a 100kN Instron 8801 servo-hydraulic testing machine equipped with an environmental chamber, as shown in Fig. 6. Before the tests, the specimens were maintained at the testing temperature in a free mode for about 45 min to achieve a temperature balance throughout the specimens.
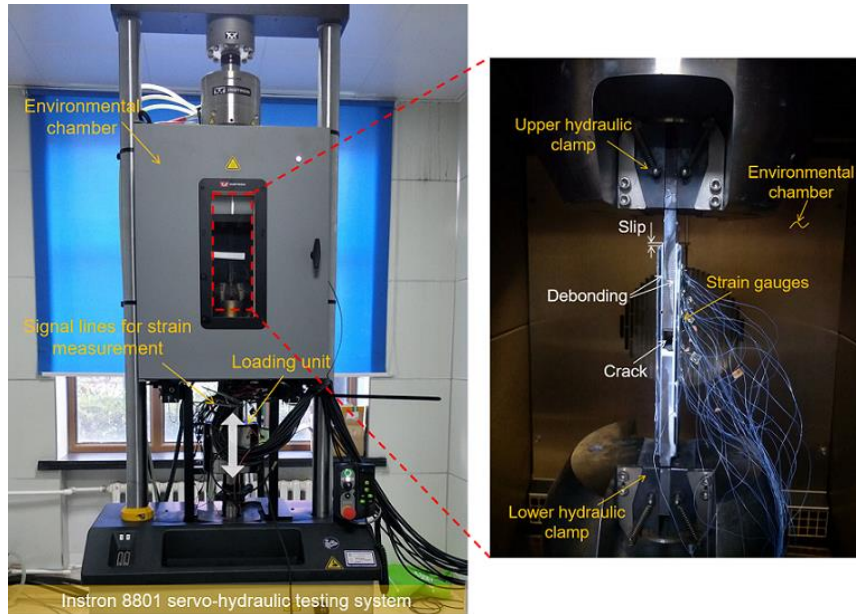
8

Fig. 6. Experimental set-up.

3.3. Loading procedure

The specimens were subjected to a sinusoidal fatigue load with a constant frequency of 16 Hz and a stress ratio of 0.4. The fatigue loading wave ranges from 24 kN to 60 kN. The maximum nominal stress in the bare specimens is 150 MPa, 33% of the steel yield strength. The tests were stopped until the relative displacement of the specimen reached 3 mm. To facilitate the measurement of crack length, we adopted the "beach marking" technique to yield beaches on the fracture surface [41, 49]. Thus, the loading cycle includes a normal fatigue loading part and a short beach marking part, as depicted in Fig. 7. In the beach marking series, a sinusoidal load from 33 kN to 51 kN is adopted.
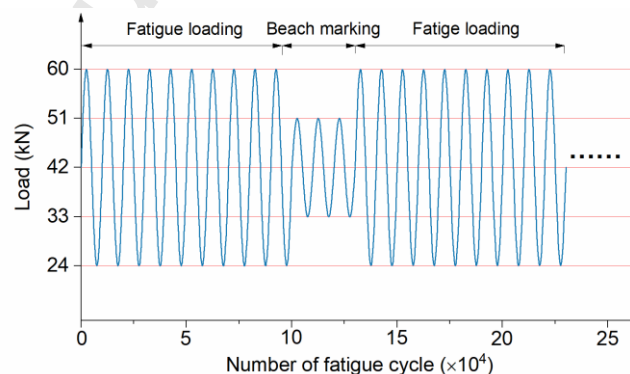

Fig. 7. Loading procedure for the fatigue tests.

3.4. Strain measurement

To monitor the damages or debonding within the adhesive layer, we glued strain gauges on the surface of CFRP to measure the strains during fatigue tests. The strain gauges were arranged to form a matrix, as shown in Fig. 8. During the fatigue tests, a static force of

9

0.5P_{max} (i.e., 30 kN) is exerted to the specimens under multi-stage loading, and the strains were measured at each loading stage. The relatively small load 30 kN was used because no damage initiation within the adhesive layer was expected under the static loading.
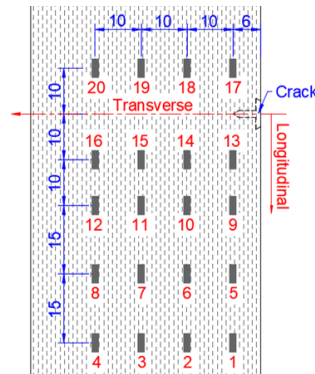

Fig. 8. Arrangement of strain gauges on CFRP (unit: mm)

4. Experimental results

The test results including the failure modes, fatigue fractures, fatigue crack growth in steel plates, and damage evolution within the bonding interface are presented here to evaluate the temperature effects on the failure process and fatigue life enhancement.

4.1. Failure characteristics of bonding interface

The fatigue test results are listed in Table 3, including the fatigue cycles to failure and the failure modes.

Table 3 Fatigue test results

Series	Specimen label	Reinforcement ratio	Cycles to failure ($\times 10^4$)	Average cycles to failure ($\times 10^4$)	Failure mode
Steel	Steel-1	0	21.3	21.7	−
	Steel-2	0	22.1		−
F1.4	F1.4-25-1	0.28	148.1	154.2	a
	F1.4-25-2	0.28	160.2		a
	F1.4-45-1	0.28	120.0	134.5	a
	F1.4-45-2	0.28	149.0		a
	F1.4-60-1	0.28	101.6	109.3	a
	F1.4-60-2	0.28	117.0		a
F3.0	F3.0-25-1	0.60	309.0	333.7	a+b
	F3.0-25-2	0.60	358.3		a+b
	F3.0-45-1	0.60	278.0	236.3	b
	F3.0-45-2	0.60	194.6		b
	F3.0-60-1	0.60	57.1	67.6	b
	F3.0-60-2	0.60	78.0		b
F3.0-1.5	F3.0-60-1.5h-1	0.60	93.6	106.7	b+a
	F3.0-60-1.5h-2	0.60	119.8		b

Notes: 1. failure mode a: CFRP/adhesive layer debonding; failure mode b: steel/adhesive layer debonding. 2. The failure mode before '+' is the dominant one.

10

The typical failure modes are shown in Fig. 9. It shows that the typical interfacial failure modes for CFRP-strengthened steel plates under fatigue loading include CFRP/adhesive layer debonding (mode a) and steel/adhesive layer debonding (mode b). In general, the failure exhibits in different modes for different CFRP materials and testing temperatures. Despite different temperatures the specimens are exposed to, all F1.4-strengthened specimens failed with the same mode (i.e. mode a), with a layer of carbon fibers remaining on the surface of the adhesive. This failure, in fact, is the superficial delamination of CFRP laminates, and no CFRP rupture occurred. It does not cause obvious damage to the stiffness of the CFRP laminates. Therefore, this failure mode can be regarded as mode a [12]. In contrast, the F3.0-strengthened specimens exhibit different failure modes at different testing temperatures. The increase in temperature leads to a failure mode transition from a+b mixed mode (at 25℃) to pure mode b (at 45℃–60℃). This means the CFRP/adhesive bonding interface is the weakest link for F1.4-strengthened specimens at all testing temperatures. However, the weakest link of F3.0-strengthened specimens transferred from the CFRP/adhesive bond to the adhesive/steel bond when the temperature exceeds 45℃. It also indicates that, as the temperature increases from 25℃ to 60℃, the adhesive/steel bond degrades faster than the CFRP/adhesive bond for the F3.0-strengthened specimens.

(a)

(b)
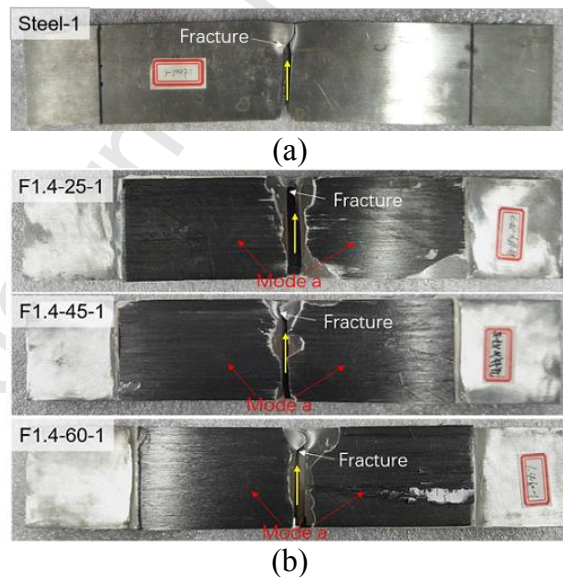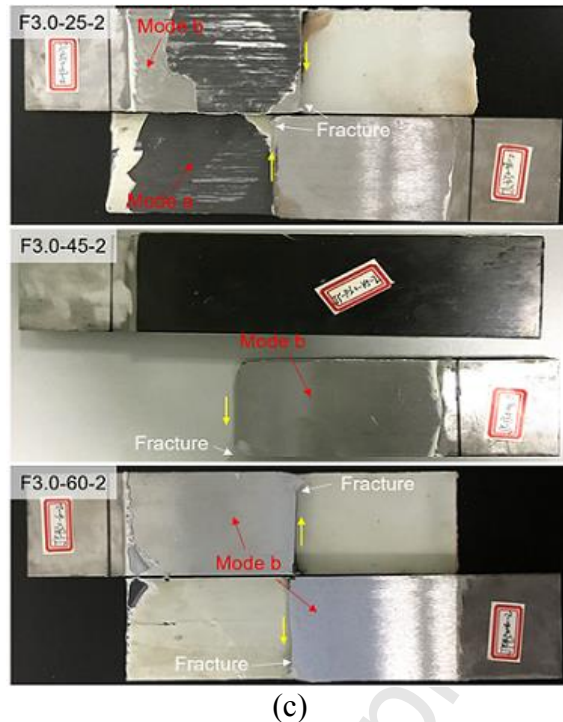
(c)

Fig. 9. Failure characteristics for (a) bare, (b) F1.4-strengthened, and (c) F3.0-strengthened specimens. Note: the yellow arrows denote the direction of fatigue crack propagation.

4.2. Fatigue fracture analysis

Based on the "beach marking" technique, the fatigue crack fronts can be observed on the fracture surfaces of the steel elements. The fatigue crack fronts on the fracture surfaces of typical specimens, taking bare specimens and F1.4-strengthened specimens as examples, are shown in Fig. 10. The results show that the "beach marking" loading intermittent produce clear crack fronts on the fracture surfaces. The fatigue and fracture process can be divided into three stages, i.e., crack initiation, crack propagation and final fracture. After being reinforced by CFRPs, more crack fronts are formed during the fatigue tests. With the increase of temperatures (from Fig. 10(b) to (d)), the fatigue crack fronts become sparser. In addition, the areas of direct fracture are varied due to applying strengthening and different temperatures. Among all these specimens, fracture area on the bare specimen steel-1 is the largest. For the CFRP-strengthened specimens, the area of direct fracture surface on specimen F1.4-60-1 is the largest, while no direct fracture surface was observed on specimen F1.4-25-1. It indicates that the CFRP strengthening also enhances the resistance against direct fracture of the steel elements, and the high-temperature for sure has an adverse influence on the fatigue life enhancement.
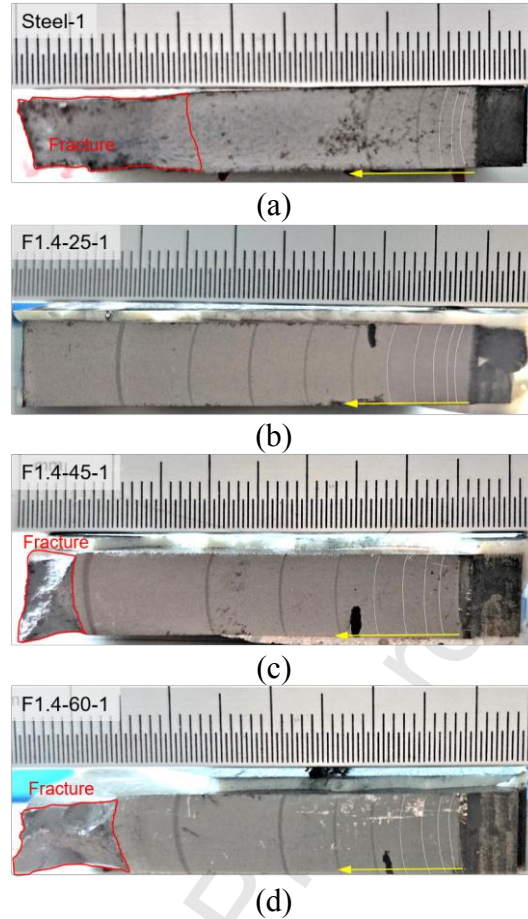
(a)

(b)

(c)

(d)

Fig. 10. Beach marks on the fracture surface. Note: the yellow arrows denote the direction of fatigue crack propagation.

4.3. Fatigue crack growth and fatigue life enhancement

The fatigue tests were terminated when the relative displacement between the two gripping ends reached 3 mm. However, all the specimens failed under cyclic loading before the displacement reached 3 mm. The numbers of fatigue cycles at failure listed in Table 2 are the actual fatigue lives of the specimens. To evaluate the fatigue enhancement effects of CFRP on the SENT specimens, the ratio of fatigue lives of strengthened specimens, N_s, to those of bare specimens, N_b, is defined as the fatigue life enhancement factor, R_N:

$$R_N = \frac{N_s}{N_b} \tag{5}$$

The fatigue crack lengths were measured by the software Image J 1.48v. The fatigue test results for all the specimens, including the fatigue crack propagations versus the number of fatigue cycles and the fatigue life enhancement factors, are plotted in Fig. 11. The crack length in this figure is the propagating crack length under the fatigue loading, excluding the initial crack length.

The results demonstrate that the CFRP strengthening can effectively delay the fatigue

13

crack propagation of notched steel elements. The overall trend is that the fatigue cracks propagation is slow at first and then accelerates. An important finding is that the fatigue crack propagations are less effectively delayed by the bonded CFRPs at the elevated temperature. At a specific temperature of 25℃ or 45℃, it is found that the 3.0 mm-thick CFRPs are more effective in delaying the fatigue crack growth than the 1.4 mm-thick CFRPs. Unexpectedly, at 60℃, the 3.0 mm-thick CFRPs are less effective in crack arresting than 1.4 mm-thick CFRPs. It may be caused by the premature debonding between the adhesive layer and steel at 60℃ (as clarified in Section 4.1). It is worth mentioning that the fatigue crack growths of the CFRP-strengthened specimens are still significantly influenced by the ambient temperatures, although these temperatures are below the glass transition temperature of the adhesive. It is also found that extending the curing duration from 1.0h to 1.5h has positive effects on the fatigue enhancement at a high temperature of 60℃.

The results in Fig. 11(b) further demonstrate that the largest R_N at room temperatures is 15.38, which is achieved by the F3.0 strengthening. However, the largest R_N at 60℃ is 5.04, which is achieved by F1.4 strengthening. It is clear that the elevated temperatures significantly reduced the values of R_N, although the environmental temperatures (25–60℃) are below the glass transition temperature of the epoxy adhesive (T_g = 66.3℃). In the study of Feng et al. [41], two-layer CFRP sheets (one-layer thickness is 0.163 mm) and epoxy resin E2500S were used to strengthen cracked steel plates. The R_N values at 20℃ and 60℃ are respectively 3.4 and 2.0, which are less than the ones in this study. It demonstrates that the selected epoxy adhesive and CFRP laminate are more effective for enhancing the fatigue performance of damaged steel structures.
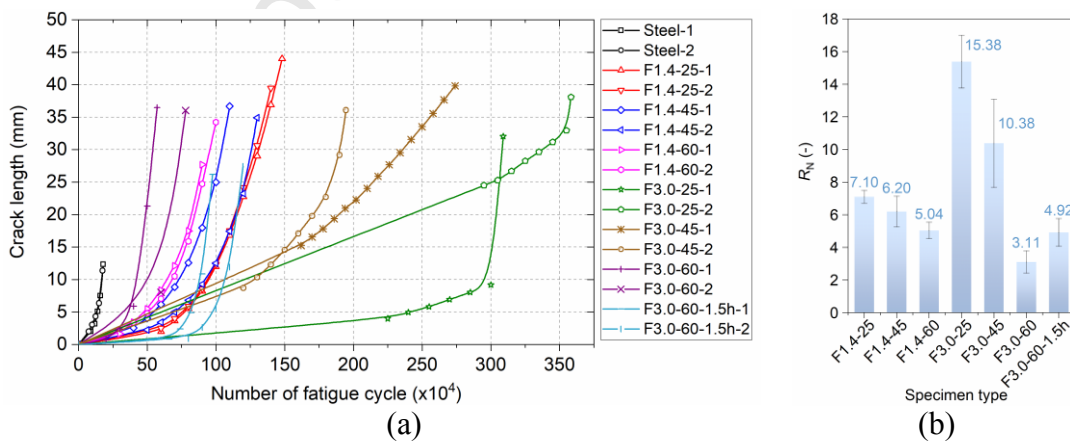

Fig. 11. Fatigue test results: (a) fatigue crack length versus number of fatigue cycles; (b) fatigue life enhancement factor.

4.4. Bonding interface damage propagation

The damage propagation within the adhesive layer can be characterized by the strain

14

changes on CFRP laminates. Here, we define the ratio of the CFRP strain after a specific number of loading cycle to the initial strain as the strain variation coefficient (SVC), as expressed by

$$SVC = \frac{\varepsilon_n}{\varepsilon_0} \tag{6}$$

where ε_n and ε_0 are the CFRP strain after a specific number of fatigue cycles and the initial strain before the test, respectively.

Fig. 12 presents the SVC evolutions at each measuring point and 3–D distributions with the increase of fatigue cycles. The longitudinal and transverse coordinates in this figure are respectively defined in Fig. 8. The results show that the SVC evolutions for the four typical specimens are different. For the F1.4-strengthened specimens at 25℃ and 60℃, the strains at almost all measuring points increased with the increase of fatigue cycles. It indicates that the force shared by the CFRPs increases as the fatigue crack continues to propagate. Before the specimen failure, the strains (characterized by SVC) around the crack opening, e.g. measuring points #13–14 and #17–18, increased to the largest. However, the debonding of CFRPs has not occurred before specimen failure. It is because the SVC will decrease if debonding occurs. For specimen F3.0-25-1, the SVCs of all strain gauges remained around one with the increasing number of cycles until the failure of the specimen. It means that no significant strain concentrations, i.e., no obvious damage, were produced before the specimen failure. The SVCs at the measuring points near the crack opening decreased greatly just before the specimen failure (as shown in Fig. 12 (c)). It shows that the debonding of CFRP (i.e. the steel/adhesive layer debonding as shown in Fig. 9(c)) occurred before the specimen failure. For specimen F3.0-60-1, the SVCs at measuring points #13 and #9 (near the crack opening) increased significantly, indicating that the stresses shared by the CFRP increased. In contrast, the SVCs at measuring points #20 and #16 (close to the final fracture surface of the crack) decreased significantly, showing that localized debonding occurred at these sites. In general, the bonding interfaces between the CFRP and steel for most specimens, although have local damage, can almost remain intact until the specimen failure, while those of the specimen F3.0-60-1 experienced premature debonding during the fatigue tests.
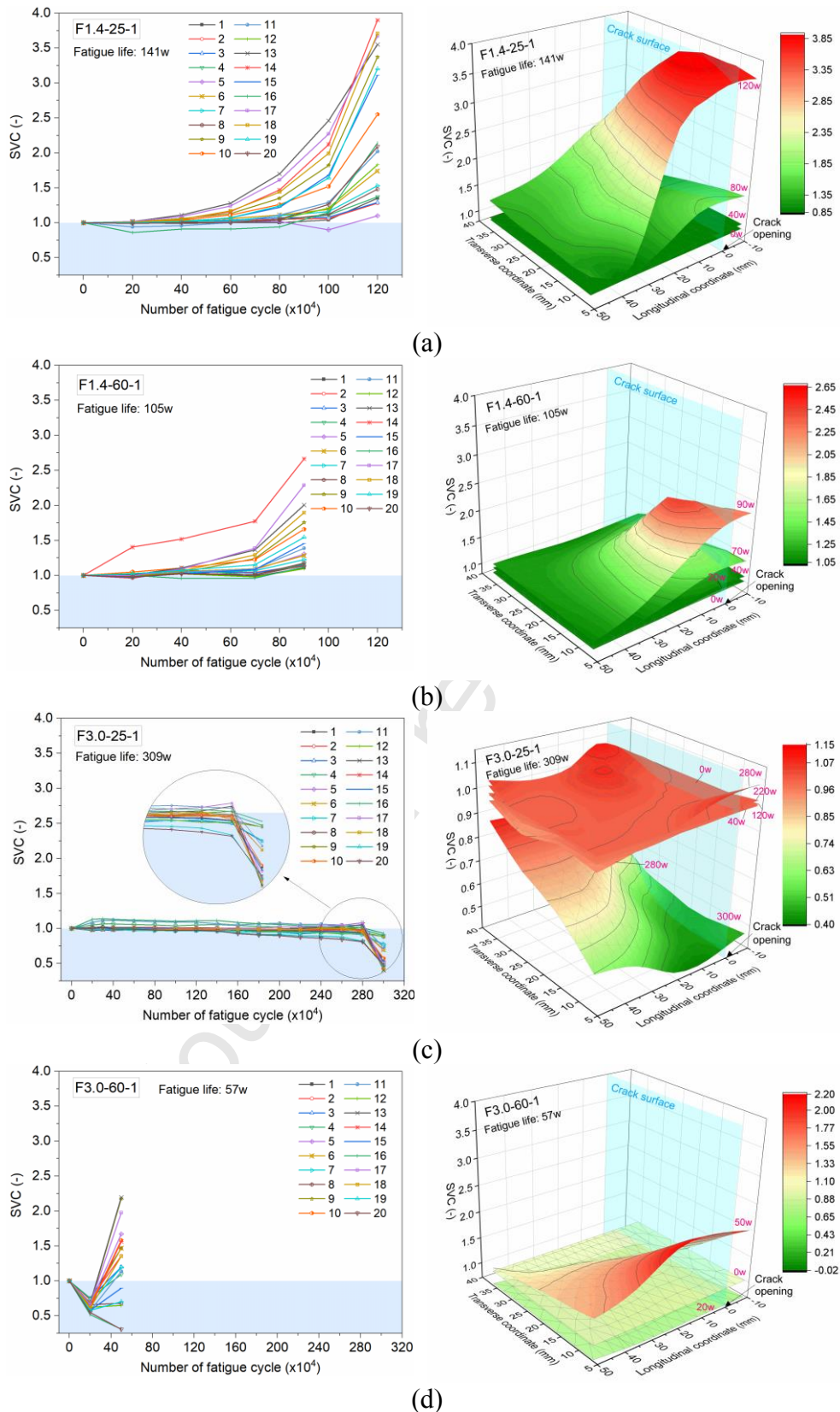
(a)

(b)

(c)

(d)

Fig. 12. SVC evolutions (left) and representative SVC 3-D distributions (right) versus number of fatigue cycles: (a) F1.4-25-1; (b) F1.4-60-1; (c) F3.0-25-1; (d) F3.0-60-1. Note: in the right-side figures, 'w' means '$\times 10^4$ cycles'.

16

5. Conclusions

This paper investigated the fatigue enhancement of damaged steel plates using epoxy-bonded CFRP patches considering the effects of elevated temperatures. The following conclusions can be drawn.

(1) The epoxy adhesive and CFRP laminas are sensitive to elevated temperatures in terms of their mechanical behaviors, which should be given serious concern in the design. Curing the epoxy adhesive layer at a moderately high temperature for a certain duration is effective to enhance its high-temperature resistance.

(2) Under the fatigue loading, the failure mode of F1.4-strengthened specimens is consistent at the temperatures from 25℃ to 60℃, i.e., the CFRP/adhesive layer debonding. The failure of F3.0-strengthened specimens transferred from the CFRP/adhesive layer debonding at 25℃ to the adhesive layer/steel debonding with the temperature exceeding 45℃.

(3) The bonded CFRP system effectively enhances the fatigue performance of damaged steel elements. However, and the elevated temperatures significantly degrade the fatigue behavior of the CFRP-strengthened specimens. The largest fatigue life enhancement factor at room temperatures is 15.38, which is achieved by the bonded 3.0 mm-thick CFRPs. The largest fatigue life enhancement factor at 60℃ is 5.04, which is achieved by the 1.4 mm-thick CFRPs. The selected epoxy adhesive and CFRP laminate are more effective than previously used adhesive and CFRP sheet for enhancing the fatigue performance of damaged steel components.

(4) The bonding interfaces between the CFRP and steel for most specimens, although have local damage, can almost remain intact during the fatigue tests. However, the high temperature of 60℃ can cause premature debonding of CFRPs for the F3.0-strengthened steel specimens, which heavily degrades their fatigue performance.

CRediT authorship contribution statement

Lu Ke: Conceptualization, Methodology, Software, Formal analysis, Writing- Original draft preparation. **Chuanxi Li:** Project administration, Conceptualization, Supervision. **Jun He:** Conceptualization, Validation. **Qiang Shen:** Software, Writing- Reviewing and Editing. **Yongming Liu:** Writing- Reviewing and Editing. **Yang Jiao:** Supervision, Writing- Reviewing and Editing.

Declaration of competing interest

The authors declare that they have no known competing financial interests or personal relationships that could have appeared to influence the work reported in this paper.

Acknowledgements

Data availability

The raw/processed data required to reproduce these findings cannot be shared at this time due to technical or time limitations.

References

[1] E. Ghafoori, M. Motavalli, Normal, high and ultra-high modulus carbon fiber-reinforced polymer laminates for bonded and un-bonded strengthening of steel beams, Mater. Design 67 (2015) 232-43. https://doi.org/10.1016/j.matdes.2014.11.031.

[2] Q. Yu, Y. Wu, Fatigue retrofitting of cracked steel beams with CFRP laminates, Compos. Struct. 192 (2018) 232-244. https://doi.org/10.1016/j.compstruct.2018.02.090.

[3] Q. Liu, J. Ma, L. Kang, G. Sun, Q. Li, An experimental study on fatigue characteristics of CFRP-steel hybrid laminates, Mater. Design 88 (2015) 643-650. https://doi.org/10.1016/j.matdes.2015.09.024.

[4] C. Wang, M. Zhai, L. Duan, Y. Wang, Cold reinforcement and evaluation of steel bridges with fatigue cracks, J. Bridge Eng 23 (2018) 04018014. https://doi.org/10.1061/(ASCE)BE.1943-5592.0001219.

[5] M.R. Ayatollahi, S.M.J. Razavi, M.Y. Yahya, Mixed mode fatigue crack initiation and growth in a CT specimen repaired by stop hole technique, Eng. Fract. Mech. 145 (2015) 115-127. https://doi.org/10.1016/j.engfracmech.2015.03.027.

[6] M. Motaleb, W. Lindquist, A. Ibrahim, R. Hindi, Repair assessment for distortion-induced fatigue cracks in a seismically retrofitted double-deck bridge complex, Eng. Struct. 183 (2019) 124-134. https://doi.org/10.1016/j.engstruct.2019.01.004.

[7] M.A. Hosen, M.Z. Jumaat, A.B.M.S. Islam, Side Near Surface Mounted (SNSM) technique for flexural enhancement of RC beams, Mater. Design 83 (2015) 587-597. https://doi.org/10.1016/j.matdes.2015.06.035.

[8] X. Wang, J. Ahn, J. Lee, B.R.K. Blackman, Investigation on failure modes and mechanical properties of CFRP-Ti6Al4V hybrid joints with different interface patterns using digital image correlation, Mater. Design 101 (2016) 188-196. https://doi.org/10.1016/j.matdes.2016.04.005.

[9] L. Ke, C. Li, N. Luo, J. He, Y. Jiao, Y. Liu, Enhanced comprehensive performance of bonding interface between CFRP and steel by a novel film adhesive, Compos. Struct. 229 (2019) 111393. https://doi.org/10.1016/j.compstruct.2019.111393.

18

[10] M.R. Irshidat, M.H. Al-Saleh, H. Almashagbeh, Effect of carbon nanotubes on strengthening of RC beams retrofitted with carbon fiber/epoxy composites, Mater. Design 89 (2016) 225-234. https://doi.org/10.1016/j.matdes.2015.09.166.

[11] F. Benyahia, L. Aminallah, A. Albedah, B. Bachir Bouiadjra, T. Achour, Experimental and numerical analysis of bonded composite patch repair in aluminum alloy 7075 T6, Mater. Design 73 (2015) 67-73. https://doi.org/10.1016/j.matdes.2015.02.009.

[12] C. Li, L. Ke, J. He, Z. Chen, Y. Jiao, Effects of mechanical properties of adhesive and CFRP on the bond behavior in CFRP-strengthened steel structures, Compos. Struct. 211 (2019) 163-174. https://doi.org/10.1016/j.compstruct.2018.12.020.

[13] M. Heshmati, R. Haghani, M. Al-Emrani, Environmental durability of adhesively bonded FRP/steel joints in civil engineering applications: State of the art, Composites Part B: Engineering 81 (2015) 259-275. https://doi.org/10.1016/j.compositesb.2015.07.014.

[14] C. Batuwitage, S. Fawzia, D. Thambiratnam, R. Al-Mahaidi, Durability of CFRP strengthened steel plate double-strap joints in accelerated corrosion environments, Compos. Struct. 160 (2017) 1287-1298. https://doi.org/10.1016/j.compstruct.2016.10.101.

[15] Y. Bai, T.C. Nguyen, X.L. Zhao, R. Al-Mahaidi, Environment-assisted degradation of the bond between steel and carbon-fiber-reinforced polymer, J. Mater. Civil Eng. 26 (2014) 04014054. https://doi.org/10.1061/(ASCE)MT.1943-5533.0000951.

[16] H.C. Biscaia, P. Ribeiro, A temperature-dependent bond-slip model for CFRP-to-steel joints, Compos. Struct. 217 (2019) 186-205. https://doi.org/10.1016/j.compstruct.2019.03.019.

[17] T. Nguyen, Y. Bai, X. Zhao, R. Al-Mahaidi, Mechanical characterization of steel/CFRP double strap joints at elevated temperatures, Compos. Struct. 93 (2011) 1604-1612. https://doi.org/10.1016/j.compstruct.2011.01.010.

[18] A. Al-Shawaf, X. Zhao, Adhesive rheology impact on wet lay-up CFRP/steel joints' behaviour under infrastructural subzero exposures, Composites Part B: Engineering 47 (2013) 207-219. https://doi.org/10.1016/j.compositesb.2012.11.012.

[19] M. Heshmati, R. Haghani, M. Al-Emrani, Durability of bonded FRP-to-steel joints: Effects of moisture, de-icing salt solution, temperature and FRP type, Composites Part B: Engineering 119 (2017) 153-167. https://doi.org/10.1016/j.compositesb.2017.03.049.

[20] T. Nguyen, Y. Bai, X. Zhao, R. Al-Mahaidi, Effects of ultraviolet radiation and associated elevated temperature on mechanical performance of steel/CFRP double strap joints, Compos. Struct. 94 (2012) 3563-3573. https://doi.org/10.1016/j.compstruct.2012.05.036.

[21] H. Jiang, Y. Cong, X. Zhang, G. Li, J. Cui, Fatigue degradation after salt spray ageing of electromagnetically riveted joints for CFRP/Al hybrid structure, Mater. Design 142 (2018) 297-307. https://doi.org/10.1016/j.matdes.2018.01.047.

[22] L. Pan, W. Ding, W. Ma, J. Hu, X. Pang, F. Wang, J. Tao, Galvanic corrosion protection and durability of polyaniline-reinforced epoxy adhesive for bond-riveted joints in AA5083/Cf/Epoxy laminates, Mater. Design 160 (2018) 1106-1116. https://doi.org/10.1016/j.matdes.2018.10.034.

[23] Y. Yang, M.A.G. Silva, H. Biscaia, C. Chastre, Bond durability of CFRP laminates-to-steel joints subjected to freeze-thaw, Compos. Struct. 212 (2019) 243-258. https://doi.org/10.1016/j.compstruct.2019.01.016.

[24] L. Ke, C. Li, J. He, S. Dong, C. Chen, Y. Jiao, Effects of elevated temperatures on mechanical behavior of epoxy adhesives and CFRP-steel hybrid joints, Compos. Struct. (2019) 111789.

https://doi.org/https://doi.org/10.1016/j.compstruct.2019.111789.

[25] J.P. Firmo, M.G. Roquette, J.R. Correia, A.S. Azevedo, Influence of elevated temperatures on epoxy adhesive used in CFRP strengthening systems for civil engineering applications, Int. J. Adhes. Adhes. 93 (2019) 8-18. https://doi.org/10.1016/j.ijadhadh.2019.01.027.

[26] P. Colombi, G. Fava, L. Sonzogni, Fatigue crack growth in CFRP-strengthened steel plates, Composites Part B: Engineering 72 (2015) 87-96. https://doi.org/10.1016/j.compositesb.2014.11.036.

[27] H. Wang, G. Wu, Y. Pang, Theoretical and numerical study on stress intensity factors for FRP-strengthened steel plates with double-edged cracks, Sensors-Basel 18 (2018) 2356. https://doi.org/10.3390/s18072356.

[28] E. Lepretre, S. Chataigner, L. Dieng, L. Gaillet, Fatigue strengthening of cracked steel plates with CFRP laminates in the case of old steel material, Constr. Build. Mater. 174 (2018) 421-432. https://doi.org/10.1016/j.conbuildmat.2018.04.063.

[29] B. Do, A. Lenwari, Empirical stress intensity factor equations for cracked steel plates repaired with double-sided FRP patches, IOP Conference Series: Materials Science and Engineering 371 (2018) 1-10. https://doi.org/10.1088/1757-899X/371/1/012056.

[30] T. Chen, L. Li, N. Zhang, X. Song, Y. Hidekuma, Fatigue performance test on inclined central cracked steel plates repaired with CFRP strand sheets, Thin Wall. Struct. 130 (2018) 414-423. https://doi.org/10.1016/j.tws.2018.06.004.

[31] J. Li, J. Deng, Y. Wang, J. Guan, H. Zheng, Experimental study of notched steel beams strengthened with a CFRP plate subjected to overloading fatigue and wetting/drying cycles, Compos. Struct. 209 (2019) 634-643. https://doi.org/10.1016/j.compstruct.2018.11.020.

[32] T. Chen, X. Gu, M. Qi, Q. Yu, Experimental study on fatigue behavior of cracked rectangular hollow-section steel beams repaired with prestressed CFRP plates, J. Compos. Constr. 22 (2018) 04018034. https://doi.org/10.1061/(ASCE)CC.1943-5614.0000872.

[33] H. Kazem, Y. Zhang, S. Rizkalla, R. Seracino, A. Kobayashi, CFRP shear strengthening system for steel bridge girders, Eng. Struct. 175 (2018) 415-424. https://doi.org/10.1016/j.engstruct.2018.08.038.

[34] H. Fang, Y. Bai, W. Liu, Y. Qi, J. Wang, Connections and structural applications of fibre reinforced polymer composites for civil infrastructure in aggressive environments, Composites Part B: Engineering 164 (2019) 129-143. https://doi.org/10.1016/j.compositesb.2018.11.047.

[35] G.A. Riveros, H. Mahmoud, C.M. Lozano, Fatigue repair of underwater navigation steel structures using Carbon Fiber Reinforced Polymer (CFRP), Eng. Struct. 173 (2018) 718-728. https://doi.org/10.1016/j.engstruct.2018.07.016.

[36] C.M. Lozano, G.A. Riveros, Effects of adhesive bond-slip behavior on the capacity of innovative FRP retrofits for fatigue and fracture repair of hydraulic steel structures, Materials 12 (2019) 1495. https://doi.org/10.3390/ma12091495.

[37] G. Qin, J. Na, W. Mu, W. Tan, J. Yang, J. Ren, Effect of continuous high temperature exposure on the adhesive strength of epoxy adhesive, CFRP and adhesively bonded CFRP-aluminum alloy joints, Composites Part B: Engineering 154 (2018) 43-55. https://doi.org/10.1016/j.compositesb.2018.07.059.

[38] A. Al-Shawaf, R. Al-Mahaidi, X. Zhao, Effect of elevated temperature on bond behaviour of high modulus CFRP/steel double-strap joints, Australian Journal of Structural Engineering 10 (2009) 63-74. https://doi.org/10.1080/13287982.2009.11465033.

[39] H. Zhou, J.P. Torres, D. Fernando, A. Law, R. Emberley, The bond behaviour of CFRP-to-steel bonded joints with varying bond properties at elevated temperatures, Eng. Struct. 183 (2019) 1121-1133.

https://doi.org/10.1016/j.engstruct.2018.10.044.

[40] T.J. Stratford, LA Bisby, Effect of warm temperatures on externally bonded FRP strengthening, J. Compos. Constr. (2012) 235-244.

[41] P. Feng, L. Hu, X. Zhao, L. Cheng, S. Xu, Study on thermal effects on fatigue behavior of cracked steel plates strengthened by CFRP sheets, Thin Wall. Struct. 82 (2014) 311-320. https://doi.org/10.1016/j.tws.2014.04.015.

[42] Q. Yu, R. Gao, X. Gu, X. Zhao, T. Chen, Bond behavior of CFRP-steel double-lap joints exposed to marine atmosphere and fatigue loading, Eng. Struct. 175 (2018) 76-85. https://doi.org/10.1016/j.engstruct.2018.08.012.

[43] ASTM E1640-18. Standard test method for the glass transition temperature by dynamic mechanical analysis. ASTM International; 2018.

[44] J. Michels, R. Widmann, C. Czaderski, R. Allahvirdizadeh, M. Motavalli, Glass transition evaluation of commercially available epoxy resins used for civil engineering applications, Composites Part B: Engineering 77 (2015) 484-493. https://doi.org/10.1016/j.compositesb.2015.03.053.

[45] ASTM D638-14. Standard test method for tensile properties of plastics, ASTM International; 2014.

[46] ASTM E647-13a. Standard test method for measurement of fatigue crack growth rates, ASTM International; 2014.

[47] X.W. Liao, Y.Q. Wang, X.D. Qian, Y.J. Shi, Fatigue crack propagation for Q345qD bridge steel and its butt welds at low temperatures, Fatigue Fract. Eng. M. 41 (2018) 675-687. https://doi.org/10.1111/ffe.12727.

[48] Z. Ding, X. Wang, Z. Gao, S. Bao, An experimental investigation and prediction of fatigue crack growth under overload/underload in Q345R steel, Int. J. Fatigue 98 (2017) 155-166. https://doi.org/10.1016/j.ijfatigue.2017.01.024.

[49] Q.Q. Yu, T. Chen, X.L. Gu, X.L. Zhao, Z.G. Xiao, Fatigue behaviour of CFRP strengthened steel plates with different degrees of damage, Thin Wall. Struct. 69 (2013) 10-17. https://doi.org/10.1016/j.tws.2013.03.012.

Graphical abstract
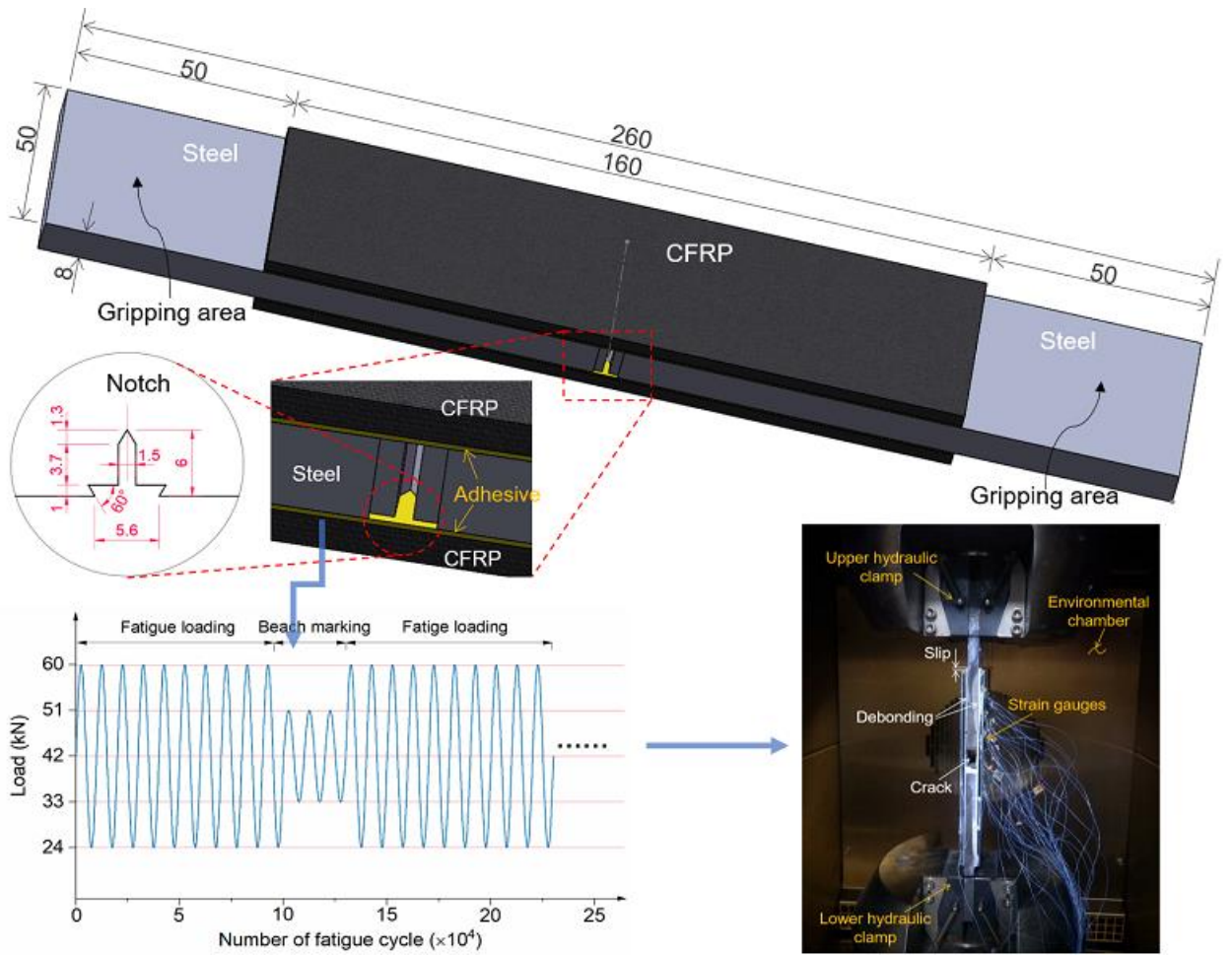
Highlights

- Curing of epoxy adhesive at elevated temperatures for a specific duration effectively enhances its high-temperature resistance.

- Properly cured bonded CFRP patches effectively enhances the fatigue performance of damaged steel structures.

- Elevated temperatures can cause failure mode transform of bonding interface between CFRP and steel.

- Elevated temperatures significantly degrade the fatigue behavior of the CFRP-strengthened steel components.

23